Acta Geotechnica (2020) 15:2969–2982
https://doi.org/10.1007/s11440-020-01003-w

RESEARCH PAPER

Seismic stability analysis of a hunchbacked retaining wall under passive state using method of stress characteristics

G. Santhoshkumar[1] · Priyanka Ghosh[1]

Received: 11 July 2019 / Accepted: 29 May 2020 / Published online: 15 June 2020

Abstract

The potential use of a hunchbacked retaining wall over a conventional retaining wall under the seismic passive state is emphasised in this study employing the method of stress characteristics coupled with the modified pseudo-dynamic approach. Unlike the available studies established with the limit equilibrium or the limit analysis method where a predefined failure mechanism is assumed prior to the analysis, the failure surface is continuously traced in due course of the present analysis. The seismic stability of a hunchbacked retaining wall under the passive condition is found to be affected greatly while considering the effect of damping of the soil-wall and the phase difference of the seismic waves. A detailed parametric study is conducted considering the influence of different soil and wall parameters such as soil-wall inertia, soil friction angle, wall inclination and roughness. The present results are obtained from a rigorous computational effort without assuming a failure mechanism and found to be in good agreement with the previous studies available in the literature.

Keywords Earthquake · Earth pressure · Hunchbacked retaining wall · Method of stress characteristics · Modified pseudo-dynamic approach

Abbreviations

a_h, a_v	Horizontal and vertical seismic accelerations
B, H	Width and height of the wall
D_S, D_W	Constant damping ratio of the soil and the wall
F_N, F_T	Normal and tangential components of forces acting at the base of the wall
FS_S	Factor of safety against sliding
g	Acceleration due to gravity
H_1, H_2	Height of upper and lower part of the wall
k_h, k_v	Horizontal and vertical seismic acceleration coefficients
K_{pq1}, K_{pq2}	Passive earth pressure coefficients for upper and lower part of the wall due to surcharge
$K_{p\gamma 1}$, $K_{p\gamma 2}$	Passive earth pressure coefficients for upper and lower part of the wall due to unit weight of the soil
P_{pe1}, P_{pe2}	Lateral thrusts acting on upper and lower part of the wall due to surcharge and unit weight of the soil
P_{pq1}, P_{pq2}	Lateral thrusts acting on upper and lower part of the wall due to surcharge only
q	Uniformly distributed surcharge
Q_{HS}, Q_{VS}	Horizontal and vertical inertial forces in the backfill soil
Q_{HW}, Q_{VW}	Horizontal and vertical inertial forces in the wall
t	Time
T	Period of lateral shaking
V_{pS}, V_{sS}	Primary and shear wave velocities in the soil
V_{pW}, V_{sW}	Primary and shear wave velocities in the wall
W_S	Weight of the backfill soil
W_W	Weight of the wall
x, y	Axes in two-dimensional Cartesian coordinate system
α_1, α_2	Inclination angle for upper and lower part of the wall
δ_1, δ_2	Wall roughness at upper and lower part of the wall
ϕ	Angle of internal friction of the soil
γ, γ_c	Unit weight of the soil and the wall material

✉ Priyanka Ghosh
priyog@iitk.ac.in

[1] Department of Civil Engineering, Indian Institute of Technology, Kanpur 208 016, India

μ_b	Coefficient of base friction for the wall
σ	Distance on the Mohr stress diagram, between the centre of the Mohr circle and a point where the Coulomb's linear failure envelope intersects the σ-axis
θ	Angle made by σ_1 in a counter-clockwise sense with the positive x-axis
θ_g	Magnitude of θ along the ground surface
θ_{W1},θ_{W2}	Magnitude of θ along upper and lower part of the wall

1 Introduction

Gravity retaining walls are widely adopted structural solutions to retain the backfill soil. Using the self-weight and the base friction, such structures offer greater resistance to the lateral earth pressure exerted by the backfill soil. The stability of such an important structural element has always been a prime concern, especially under the influence of earthquakes. The prediction of earth pressure and stability of retaining walls under both static and seismic conditions was demonstrated by several researchers leading to various simplified theories [4, 5, 7, 26, 28, 30, 35, 45, 48, 49]. Mononobe–Okabe method [26, 30] is a notable theory developed in the framework of the limit equilibrium method to predict the earth pressure under the seismic condition using the pseudo-static approach. However, the assumed linear failure surface in the Mononobe–Okabe method performs better in the case of active condition, whereas in the case of passive condition the failure surface generally comes out to be nonlinear even under the static condition [27]. Hence, based on the pseudo-static approach, various theories were germinated to capture such nonlinear failure surface [20, 27, 42] behind a retaining wall, where a predefined failure mechanism was much demanded. However, Sokolovski [41] proposed the method of stress characteristics to capture the natural development of a failure surface and later, it was further explored by several researchers for different geotechnical problems [15, 21, 24, 39]. Employing the method of stress characteristics and the pseudo-static approach, Kumar and Chitikela [21] determined the seismic passive earth pressure without assuming a priori failure mechanism. However, it is commonly understood that in the pseudo-static approach, the seismic forces are assumed to pronounce a uniform acceleration throughout the disturbed soil domain. Hence, unlike the pseudo-static approach, the nonlinearity in the seismic effect was revisited by Steedman and Zeng [43] by including the time dependency and the phase effect of seismic waves in the analysis. This theory was supported by a series of centrifuge tests [50] and popularised as the original pseudo-dynamic (OPD) approach. Later, the OPD approach was utilised by several researchers to determine the seismic passive earth pressure and the bearing capacity of foundation under the seismic condition [6, 11–14, 39]. However, due to some mathematical limitations such as nonzero stress condition at the ground surface, the OPD approach was later modified as the modified pseudo-dynamic (MPD) approach by Bellezza [2] and Pain et al. [31] utilising a visco-elastic soil model along with the stress-free boundary conditions. In addition to the zero stress condition at the ground surface, the effect of frequency ratio, ground amplification and soil damping can also be admitted in the MPD approach. Recent advancements in the determination of seismic passive pressure distinctly demonstrate that either the limit equilibrium or the limit analysis is the favourable choice among the researchers for such a class of problem though it is an established fact that the assumption of a preconceived failure mechanism may not reflect the true behaviour of the backfill soil. Hence, there is a need to revisit the assumption of a predefined failure mechanism behind a retaining wall, especially under the seismic condition.

Further, the effect of soil inertia was considered to be the dominant parameter in the generation of seismic passive thrust in most of the available studies on the seismic analysis of retaining walls [6, 11, 14, 18, 20, 21, 25, 42, 49]. Though the argument is found to be quite reasonable for a cantilever retaining wall system, the effect of wall inertia cannot be neglected in the seismic design of gravity retaining walls [1, 29, 34]. However, due to bulky structure, the design of gravity retaining wall needs to be optimised well as it incurs huge construction cost. Sadrekarimi [37] explored the feasibility of using a hunchbacked retaining wall (Fig. 1a) as an effective alternative for a conventional gravity wall system (Fig. 1b) under the active condition by conducting several model tests followed by an analytical solution procedure based on the limit equilibrium method and the pseudo-static approach [38]. A hunchbacked retaining wall configuration not only alters the location of the dynamic thrust but also slashes the construction cost considerably. Among the few available studies on a hunchbacked gravity wall [32, 37, 38], none reported the performance of a retaining wall under the passive condition considering the cumulative effect of backface geometry of the wall, adaptive failure surface, soil and wall inertia force, and dynamic material properties. Hence, by employing the method of stress characteristics in association with the MPD approach, the seismic stability analysis of a hunchbacked retaining wall is performed in

the present study considering all possible inertial effects and damping ratio.

2 Problem definition

A hunchbacked gravity retaining wall of height H and top width B is considered to retain a dry, cohesionless, horizontal backfill subjected to a uniform surcharge q as shown in Fig. 2. The hunchback geometry of the wall is maintained on the backfill side by considering bilinear slopes (OO' and $O'C$), which make an angle α_1 and α_2 with the horizontal at the upper and the lower segments of the wall, respectively. δ_1 and δ_2 represent the wall roughness along the upper and the lower parts, respectively. The magnitude of wall height ratio (H_1/H_2), top wall inclination (α_1) and bottom wall inclination (α_2) are so chosen that the top width (OA) and the bottom width (CE) of the wall remain same to ensure the geometric closure. The effect of the earthquake is considered by employing the MPD approach. The seismic event was simulated by employing a harmonic base shaking with horizontal (a_h) and vertical (a_v) earthquake accelerations without causing the shear fluidisation [36]. The main objective of this study is to explore the passive resistance of a hunchbacked gravity wall under the seismic condition without assuming a predefined failure mechanism.

3 Methodology

The problem defined in this study was solved using the method of stress characteristics coupled with the MPD approach. As the solution of characteristic equations was developed in the framework of the theory of plasticity [41], the present analysis adhered to the following assumptions

i. The backfill soil is homogeneous, isotropic and obeys the Mohr–Coulomb failure criterion within the plastic shear zone.
ii. The problem is analysed under the two-dimensional plain strain condition.
iii. The principle of superposition stays legitimate so that the effect of the surcharge component can be decoupled from the passive thrust to obtain the contribution of the unit weight of the soil alone.

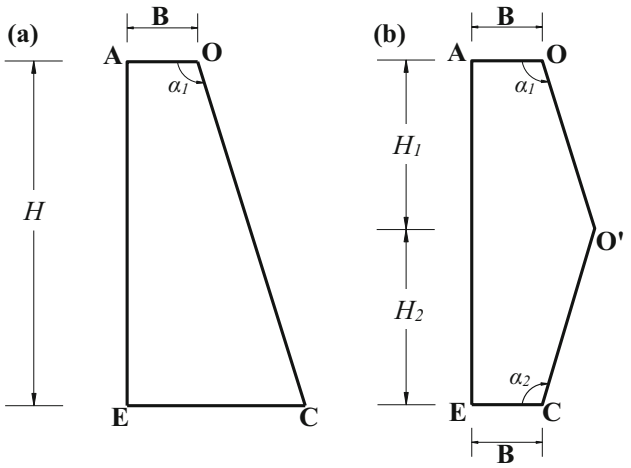

Fig. 1 Schematic representation of different retaining wall configurations; **a** conventional wall, **b** hunchbacked wall

3.1 Method of stress characteristics

The point O located at the top of the retaining wall is kept as the origin of the co-ordinate axes x–y, and their respective positive directions are illustrated in Fig. 2. The anticlockwise rotation measured from the positive x-axis is considered as positive in the whole analysis (Fig. 3a). The equations of equilibrium for a plane strain problem can be expressed as

$$\frac{\partial \sigma_x}{\partial x} + \frac{\partial \tau_{xy}}{\partial y} = X \tag{1}$$

$$\frac{\partial \tau_{xy}}{\partial x} + \frac{\partial \sigma_y}{\partial y} = Y \tag{2}$$

where σ_x, σ_y and τ_{xy} are the normal and shear stress components acting on a typical soil element as shown in Fig. 3a; X and Y are the body forces acting along the x and y directions, respectively. From the typical Mohr–Coulomb failure criterion (Fig. 3b), the stress components can be determined and expressed as

$$\sigma_x = \sigma(1 + \sin\phi\cos 2\theta) \tag{3}$$

$$\sigma_y = \sigma(1 - \sin\phi\cos 2\theta) \tag{4}$$

$$\tau_{xy} = \sigma\sin\phi\sin 2\theta \tag{5}$$

By substituting Eqs. (3), (4) and (5) in Eqs. (1) and (2), the following expressions applicable along the two different families of characteristics can be derived,

Along $(\theta-\mu)$ characteristic,

$$\frac{dy}{dx} = \tan(\theta-\mu); \frac{d\eta}{dx} = \frac{X\sin(\theta+\mu) - Y\cos(\theta+\mu)}{2\sigma\sin\phi\cos(\theta-\mu)} \tag{6}$$

Along $(\theta+\mu)$ characteristic,

$$\frac{dy}{dx} = \tan(\theta+\mu); \frac{d\xi}{dx} = -\frac{X\sin(\theta-\mu) - Y\cos(\theta-\mu)}{2\sigma\sin\phi\cos(\theta+\mu)} \tag{7}$$

where $\mu = (\pi/4 - \phi/2)$ and $\left.\begin{matrix}\eta\\ \xi\end{matrix}\right\} = 0.5\cot\phi ln\frac{\sigma}{q} \mp \theta.$

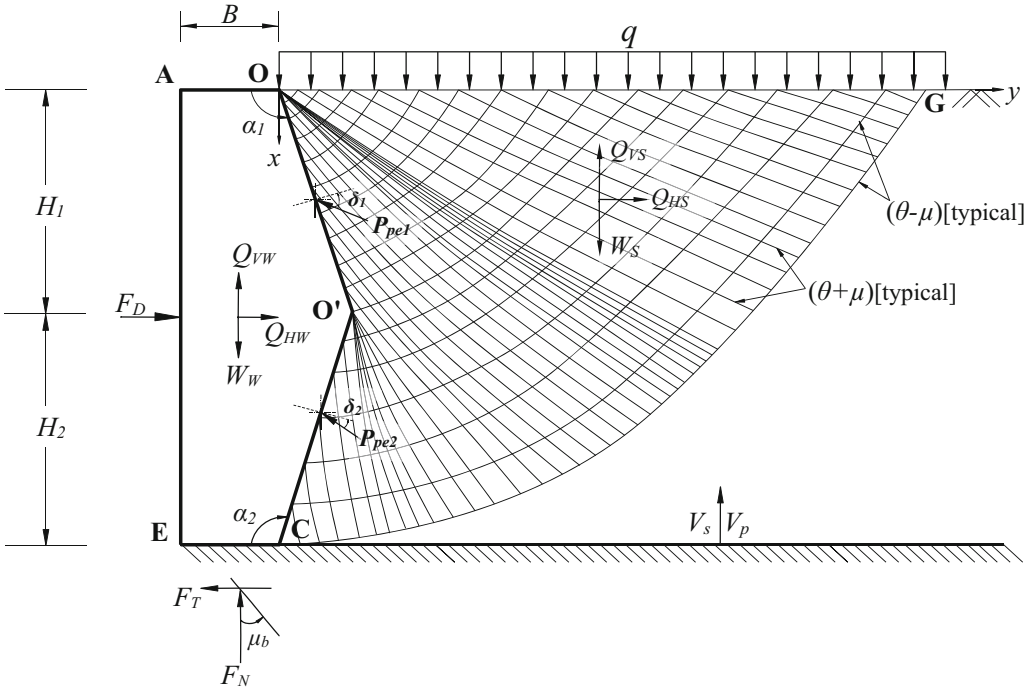

Fig. 2 Schematic representation of a hunchbacked retaining wall and associated forces

The detailed derivation of the characteristic equations can be obtained from various investigations [21, 24, 40] and hence, for the sake of brevity, the same is excluded from this paper. By generating a network of two different families of characteristics ($(\theta+\mu)$) and ($(\theta-\mu)$), a solution can be established from a known stress boundary to an unknown stress boundary, and the actual failure surface can be traced in due course of the analysis.

3.2 Seismic accelerations

Soil is generally considered as a visco-elastic material in the MPD approach, which mostly removes the limitation of the OPD approach. In this study, Kelvin–Voigt model was employed to capture the elastic and the damping component of the soil with the help of purely elastic spring and dashpot system, respectively [8]. The plane wave equations of motion propagating along the x-axis at any time t can be expressed as

$$\frac{\gamma}{g}\frac{\partial^2 u_h}{\partial t^2} = G\frac{\partial^2 u_h}{\partial x^2} + v_h\frac{\partial^3 u_h}{\partial x^2 \partial t} \tag{8}$$

$$\frac{\gamma}{g}\frac{\partial^2 u_v}{\partial t^2} = (\lambda + 2G)\frac{\partial^2 u_v}{\partial x^2} + v_v\frac{\partial^3 u_h}{\partial x^2 \partial t} \tag{9}$$

where u_v and u_h are the displacements along x and y direction, respectively; G and λ are the Lame's constants; v_h and v_v are the soil viscosities along the respective plane of motion.

By imposing the stress-free boundary condition at the ground surface, the horizontal (a_{hS}) and the vertical (a_{vS}) seismic accelerations in the soil at any depth, x and any instant, t can be obtained from Eqs. (10) and (11) [2]. The detailed derivations of Eqs. (10) and (11) are also available in several recent works [3, 31, 33, 34].

$$\begin{aligned} a_{hS}(x,t) = \frac{k_h g}{C_{sS}^2 + S_{sS}^2}\big[&(C_{sS}C_{sSx} + S_{sS}S_{sSx})\cos(\omega t) \\ &+(S_{sS}C_{sSx} - C_{sS}S_{sSx})\sin(\omega t)\big] \end{aligned} \tag{10}$$

$$\begin{aligned} a_{vS}(x,t) = \frac{k_v g}{C_{pS}^2 + S_{pS}^2}\big[&\left(C_{pS}C_{pSx} + S_{pS}S_{pSx}\right)\cos(\omega t) \\ &+\left(S_{pS}C_{pSx} - C_{pS}S_{pSx}\right)\sin(\omega t)\big] \end{aligned} \tag{11}$$

where

$$\begin{aligned} C_{sSx} &= \cos\left(\frac{y_{sS1}x}{H}\right)\cosh\left(\frac{y_{sS2}x}{H}\right); S_{sSx} \\ &= -\sin\left(\frac{y_{sS1}x}{H}\right)\sinh\left(\frac{y_{sS2}x}{H}\right) \end{aligned} \tag{12}$$

$$\begin{aligned} C_{pSx} &= \cos\left(\frac{y_{pS1}x}{H}\right)\cosh\left(\frac{y_{pS2}x}{H}\right); S_{sSx} \\ &= -\sin\left(\frac{y_{pS1}x}{H}\right)\sinh\left(\frac{y_{pS2}x}{H}\right) \end{aligned} \tag{13}$$

and,

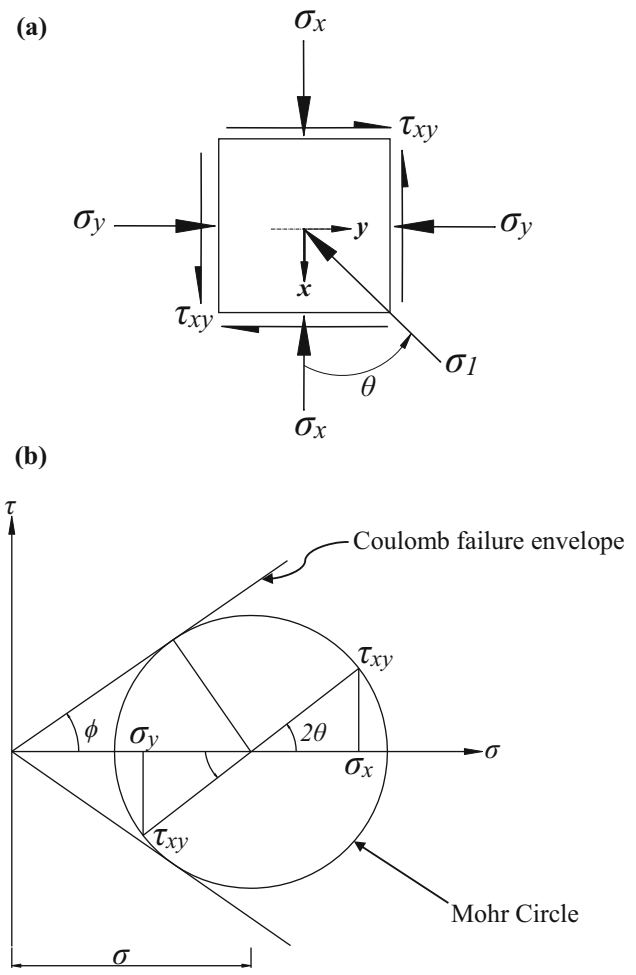

Fig. 3 Definition of stress parameters; **a** physical plane, **b** stress plane

$$y_{sS1} = \frac{\omega H}{V_{sS}}\left[\frac{\left(1+4D_S^2\right)^{0.5}+1}{2\left(1+4D_S^2\right)}\right]^{0.5}; y_{sS2} = \frac{\omega H}{V_{sS}}\left[\frac{\left(1+4D_S^2\right)^{0.5}-1}{2\left(1+4D_S^2\right)}\right]^{0.5} \quad (14)$$

$$y_{pS1} = \frac{\omega H}{V_{pS}}\left[\frac{\left(1+4D_S^2\right)^{0.5}+1}{2\left(1+4D_S^2\right)}\right]^{0.5}; y_{pS2} = \frac{\omega H}{V_{pS}}\left[\frac{\left(1+4D_S^2\right)^{0.5}-1}{2\left(1+4D_S^2\right)}\right]^{0.5} \quad (15)$$

In Eqs. (10) – (15), the first subscripts 'p' and 's' refer to the nature of the propagating waves (primary and shear waves), whereas the second subscript '$_S$' refers to the soil only. At $x = H$, the coefficients depicted in Eqs. (12) and (13) simply reduce to the constants (C_{sS}, S_{sS}, C_{pS} and S_{pS}) used in Eqs. (10) and (11). Similarly, the acceleration equations for the wall (a_{hW} and a_{vW}) can be obtained by simply replacing the second subscript '$_S$' with '$_W$' and D_S with D_W. Though the pseudo-dynamic analysis was essentially evolved from the theory of elastic wave propagation, the OPD approach was endorsed with a series of centrifuge experiments performed by Zeng and Steedman [50]. Thereafter, the OPD and the MPD approaches were widely adopted in various earth pressure-related problems [1–3, 11, 18, 31, 33, 34]. Hence, it is worth concluding at this stage that the expressions of seismic accelerations discussed in Eqs. (10–15) can be applicable to this class of problem without much deviation though they are generally derived based on the theory of elastic wave propagation. Therefore, while establishing the solution of the method of characteristics as discussed in the previous section, the effect of the earthquake can be effectively incorporated in the present analysis by admitting Eqs. (10) and (11).

3.3 Boundary conditions

Figure 2 illustrates the existence of two singular points (O and O') due to the hunchback geometry of the wall backface [21, 23, 39, 40]. From the concept of rotation of stresses at these singular points, the magnitude of θ along the ground surface (θ_g), and the upper and the lower segments of the wall (θ_{W1} and θ_{W2}) can be expressed as

$$\theta_g = 0.5\left[\pi + \kappa + \sin^{-1}\left(\frac{\sin\kappa}{\sin\phi}\right)\right] \quad (16)$$

where $\kappa = \tan^{-1}\left(\frac{a_{hS}}{g-a_{vS}}\right)$

$$\theta_{W1} = 0.5\left(2\alpha_1 - \delta_1 - \sin^{-1}\left(\frac{\sin\delta_1}{\sin\phi}\right)\right) \quad (17)$$

$$\theta_{W2} = 0.5\left(2\pi - 2\alpha_2 - \delta_2 - \sin^{-1}\left(\frac{\sin\delta_2}{\sin\phi}\right)\right) \quad (18)$$

where a_{hS} and a_{vS} are horizontal and vertical seismic accelerations in the soil, respectively, as obtained from Eqs. (10) and (11).

Based on the magnitudes of θ_g, θ_{W1} and θ_{W2}, different types of stress fields are encountered in the solution procedure. On account of the equal magnitudes of θ at the singular point, the solution becomes unique, and hence, a closed-form solution can be obtained by neglecting the unit weight of the soil [21, 40]. However, when the magnitudes of θ at the respective singular points are not equal, the effect of unit weight cannot be simply neglected due to the existence of a characteristic solution, which can only be solved using a rigorous solution procedure [21, 23, 39, 41].

3.4 Seismic lateral earth pressure

While employing the method of stress characteristics in a cohesionless soil, a nominal amount of surcharge is

generally considered to maintain the numerical stability in the analysis [21]. However, the effect of applied surcharge in the analysis may be decoupled from the final solution with the help of the principle of superposition [39]. Hence, the analysis was initially performed by considering a surcharge without accounting for the unit weight component, i.e. $q \neq 0$ and $\gamma = 0$ and the passive lateral thrusts acting on the upper (P_{pq1}) and the lower (P_{pq2}) segments of the wall were determined. Later, the analysis was carried out further by including the unit weight ($q \neq 0$ and $\gamma \neq 0$) to determine the lateral thrusts on the upper (P_{pe1}) and the lower (P_{pe2}) parts of the wall. The idealised earth pressure distribution for the latter case is shown in Fig. 4. Thus, the coefficient of seismic passive earth pressure for the upper segment of the wall due to surcharge (K_{pq1}) and unit weight ($K_{p\gamma 1}$) can be expressed as

$$K_{pq1} = \frac{P_{pq1}}{qH_1}; K_{p\gamma 1} = \frac{2\left(P_{pe1} - P_{pq1}\right)}{\gamma H_1^2} \tag{19}$$

Similarly, the coefficient of passive earth pressure for the lower segment of the wall (K_{pq2} and $K_{p\gamma 2}$) can be obtained as

$$K_{pq2} = \frac{P_{pq2}}{qH_2}; K_{p\gamma 2} = \frac{2\left(P_{pe2} - P_{pq2} - K_{pq2}\gamma H_1 H_2\right)}{\gamma H_2^2} \tag{20}$$

From Fig. 4, it can be understood that the surcharge contribution ($K_{pq2}\gamma H_1$) in Eq. (20) can be actually derived from the unit weight of the backfill soil engaged in the upper portion of the wall (H_1).

3.5 Stability analysis

A hunchbacked retaining wall needs to be displaced adequately for mobilising the passive resistance in the soil, and hence, the investigation on the seismic passive resistance numerically (finite element analysis) or experimentally is found to be practically difficult especially under a low level of seismic acceleration [47]. In this study, the stability of a hunchbacked retaining wall against the sliding mode of failure was examined using the allowable driving force (F_D), which was assumed to mobilise the full passive resistance in the system. With the known values of F_D, a hunchbacked gravity retaining wall can be effectively designed to ensure the stability of retaining structures under the seismic passive condition. Having adopted a suitable factor of safety (FS) under the seismic condition, the magnitude of F_D developed in the system can be calculated as

$$F_N = W_W - Q_{VW} - P_{pe1}\cos(\delta_1 - \alpha_1) + P_{pe2}\cos(\delta_2 - \alpha_2) \tag{21}$$

$$F_T = \mu_b F_N - P_{pe1}\sin(\delta_1 - \alpha_1) - P_{pe2}\sin(\delta_2 - \alpha_2) \tag{22}$$

$$F_D = \frac{F_T}{FS_S} - Q_{HW} \tag{23}$$

where F_N and F_T are the normal and the tangential forces acting at the base of the wall; W_W, Q_{HW} and Q_{VW} are the wall inertial forces due to self-weight, horizontal and vertical seismic accelerations, respectively, which can be obtained from the following expressions,

$$W_W = \gamma_c(AreaofAOO\prime CE) \tag{24}$$

$$Q_{HW}(t) = \int_0^{H_1} \frac{\gamma_c}{g}(B - x\cot\alpha_1)a_{hW}dx + \int_{H_1}^{H_2} \frac{\gamma_c}{g}(B - (H - x)\cot\alpha_2)a_{hW}dx \tag{25}$$

$$Q_{VW}(t) = \int_0^{H_1} \frac{\gamma_c}{g}(B - x\cot\alpha_1)a_{vW}dx + \int_{H_1}^{H_2} \frac{\gamma_c}{g}(B - (H - x)\cot\alpha_2)a_{vW}dx \tag{26}$$

where a_{hW} and a_{vW} are the accelerations caused by the seismic waves propagating through the wall material, which can be determined by performing operations similar to Eqs. (10) – (15) with appropriate wall parameters [34].

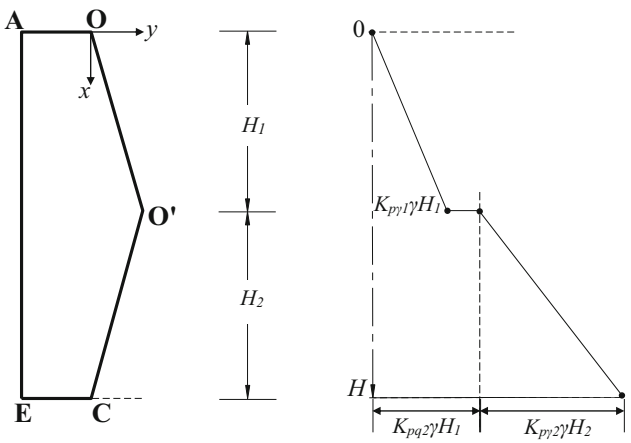

Fig. 4 Idealised earth pressure distribution behind a hunchbacked wall considering $q = 0$ and $\gamma \neq 0$

4 Results and discussion

The defined problem was solved with the aid of an in-house computer code developed in MATLAB. As mentioned earlier, a nominal value of surcharge was needed to maintain the numerical stability during the analysis. However, the contribution of surcharge component was

decoupled from the final results to obtain the contribution of the unit weight alone. Table 1 depicts the various input parameters used in the analysis. It is worth mentioning that the negative value of k_v shown in Table 1 denotes the propagation of primary waves along the negative x direction.

4.1 Passive thrust

The proposed hunchbacked gravity retaining wall counteracts the external driving force mainly using the self-weight of the wall and the seismic passive resistance offered by the backfill soil on the wall. While the inertial forces acting on the wall can be calculated from Eqs. (24), (25) and (26), the seismic passive resistance of the backfill soil can be determined from the seismic earth pressure coefficients described in Eqs. (19) and (20). The variation of seismic passive earth pressure coefficients (K_{pq1} and $K_{p\gamma 1}$) for the upper portion of the wall with the upper wall inclination (α_1) is shown in Fig. 5a. It can be observed that the passive resistance of the backfill soil decreases with an increase in the magnitude of α_1. Similarly, the variation of passive earth pressure coefficients (K_{pq2} and $K_{p\gamma 2}$ for the lower part of the wall with the lower wall inclination (α_2) is depicted in Fig. 5b. Considerable enhancement in the passive resistance of the soil can be seen with an increase in α_2. However, in any case, the magnitude of passive earth pressure coefficients is found to decrease with an increase in the seismic acceleration irrespective of the wall configuration. Hence, by adopting a retaining wall with such bilinear backface, the backfill soil can be effectively utilised to resist the driving forces under the seismic passive condition. It can also be conceived from Fig. 5 that the consideration of surcharge alone ($\gamma = 0$) generally underpredicts the passive resistance of the backfill soil, which convincingly recommends the inclusion of the self-weight of the backfill in the analysis unlike the available simplified closed form solutions [28, 40].

Table 1 Various input parameters used in the analysis

Parameter	Value
H (m)	10
B (m)	0.4H
α_1, α_2 (°)	90–110
ϕ (°)	25–40
δ_1, δ_2 (°)	0–ϕ
γ (kN/m^3)	18
γ_c (kN/m^3)	25
μ_W	0.6
D_S (%)	10
D_W (%)	5
V_{pS} (m/s)	187
V_{pW} (m/s)	3900
V_{sS} (m/s)	100
V_{sW} (m/s)	2500
T (s)	0.66
k_h	0–0.4
k_v	$-0.5k_h$ to $+k_h$

4.2 Driving force

In Fig. 6, the variation of the normalised allowable driving force ($F_D/\gamma H^2$) with different values of α_2 is presented, which actually demonstrates the stability of a hunchbacked wall against the sliding mode of failure. As mentioned earlier, a suitable factor of safety against sliding was assumed in the analysis following various standard recommendations [9, 16, 46]. Figure 6 also compares the performance of a hunchbacked (Fig. 1b) and a

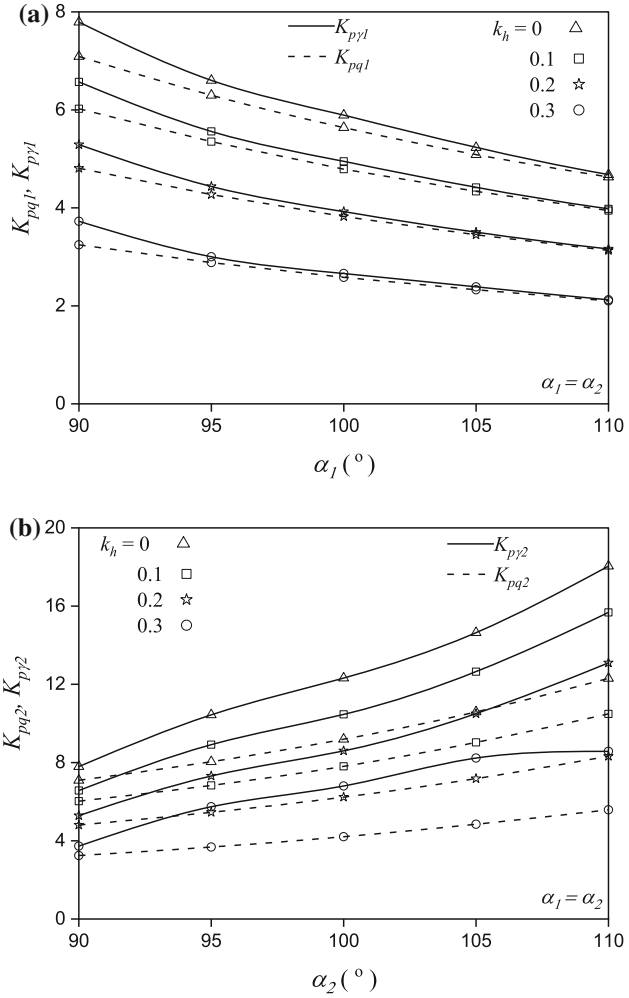

Fig. 5 Variation of **a** K_{pq1}, $K_{p\gamma 1}$, **b** K_{pq2}, $K_{p\gamma 2}$, with α_1 and α_2 for $H_1/H_2 = 1$, $\phi = 35°$, $\delta_1 = \delta_2 = 2\phi/3$, $k_v = -0.5k_h$ and $D_S = 10\%$

conventional (Fig. 1a) retaining wall against the sliding mode of failure under the seismic condition simulated by the pseudo-static as well as the modified pseudo-dynamic approaches. It can be observed that under the static as well as the seismic conditions, the magnitude of F_D (with $FS_S = 1.2$) for the hunchbacked wall is marginally higher up to a certain wall inclination (α_2) compared to the conventional wall. Figure 7 shows the variation of $F_D/\gamma H^2$ with k_h for different values of wall geometry utilising the modified pseudo-dynamic accelerations. It is worth mentioning that the extreme boundaries ($H_2 = H$ and $H_1 = H$) in Fig. 7 correspond to a conventional wall with single linear slope, whereas a hunchbacked wall is denoted by the wall height ratio (H_1/H_2). It is evident from Figs. 6 and 7 that a hunchbacked wall can perform even better by optimising the wall inclination and H_1/H_2 ratio accordingly. However, beyond a certain magnitude of H_1/H_2 ratio and α_2, the improvement in the sliding stability is found to be marginal. In Fig. 8, the variation of $F_D/\gamma H^2$ with different values of FS_S is presented. The magnitude of F_D is found to decrease with the increase in k_h and FS_S. Hence, by adopting suitable wall geometry, a hunchbacked wall can be a better alternative to a conventional wall in terms of performance and economy.

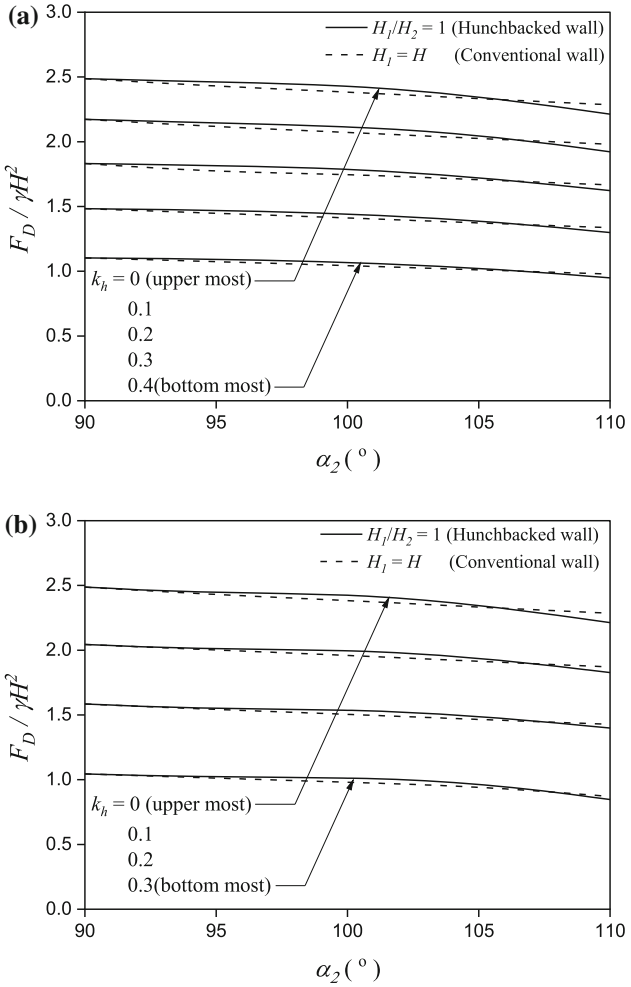

Fig. 6 Variation of $F_D/\gamma H^2$ with different values of α_2 for $\phi = 35°$, $\delta_1 = \delta_2 = 2\phi/3$, $\alpha_1 = \alpha_2$, $k_v = -0.5k_h$, $D_S = 10\%$, $D_W = 5\%$ and $FS_S = 1.2$; **a** pseudo-static approach, **b** modified pseudo-dynamic approach

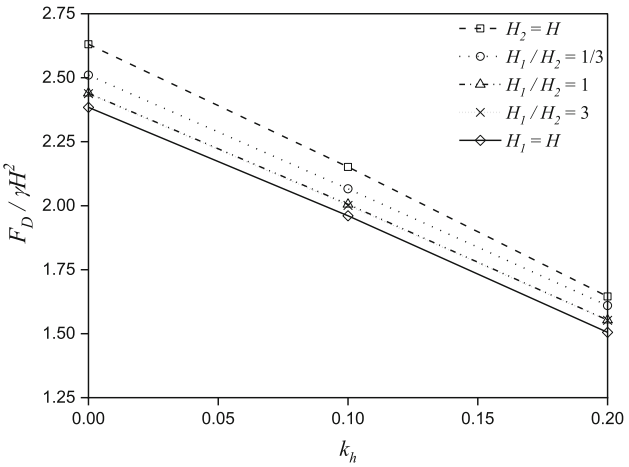

Fig. 7 Variation of $F_D/\gamma H^2$ with k_h for different wall configurations with $\phi = 35°$, $\delta_1 = \delta_2 = 2\phi/3$, $\alpha_2 = 100°$, $k_v = -0.5k_h$, $D_S = 10\%$, $D_W = 5\%$ and $FS_S = 1.2$

4.3 Soil and wall properties

From Eqs. (3) – (7), it can be understood that σ and θ are the two important parameters corresponding to the stresses and their direction, respectively. Hence, in this section, the effect of various soil and wall parameters on the seismic passive earth pressure distribution behind a hunchbacked wall is briefly discussed in terms of σ.

4.3.1 Soil friction

The comprehensive effect of ϕ on the normalised stress ($\sigma/\gamma H$) distribution behind a hunchbacked wall is shown in Fig. 9. The roughness of the upper and the lower parts of the wall is reasonably considered as two-third of the soil friction angle, that is, $\delta_1=\delta_2=2\phi 3$. From Fig. 9, it can be observed that the normalised stress increases significantly with the increase in ϕ throughout the height of the wall, similar to the observations made by earlier researchers on a conventional wall [17, 31]. However, the stress distribution is found to be significant at the lower portion of the wall.

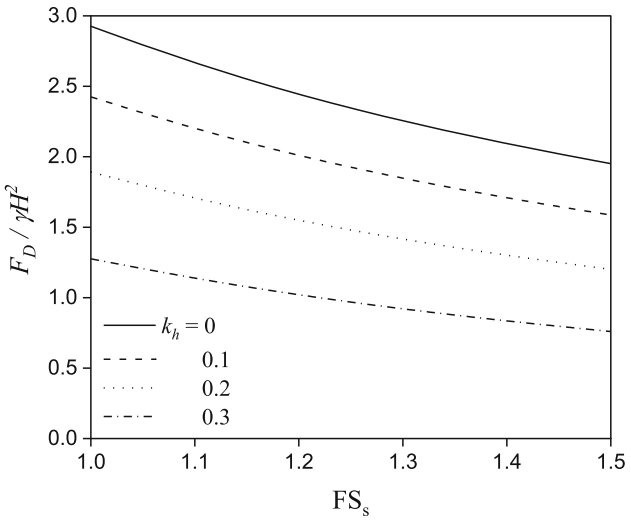

Fig. 8 Variation of $F_D/\gamma H^2$ with different values of FS_S for $\phi = 35°$, $\delta_1 = \delta_2 = 2\phi/3$, $\alpha_1 = \alpha_2 = 100°$, $H_1/H_2 = 1$, $k_h = 0.2$, $k_v = -0.5k_h$, $D_S = 10\%$ and $D_W = 5\%$

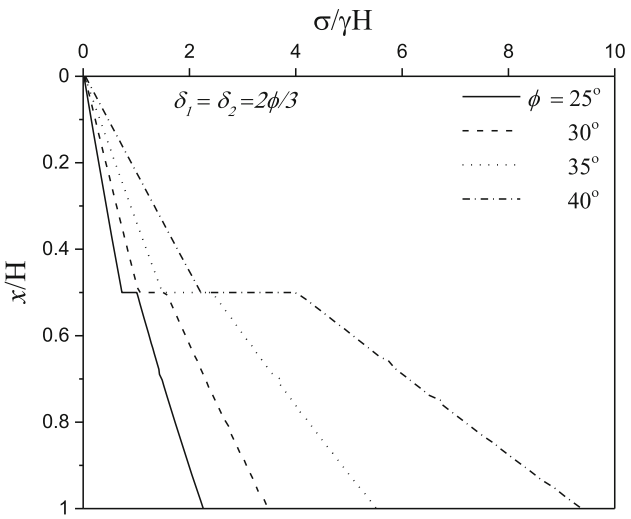

Fig. 9 Normalised stress distribution for different values of ϕ with $\delta_1 = \delta_2 = 2\phi/3$, $\alpha_1 = \alpha_2 = 100°$, $H_1/H_2 = 1$, $k_h = 0.2$, $k_v = -0.5k_h$ and $D_S = 10\%$

4.3.2 Wall roughness

Figure 10 shows the effect of wall roughness on the normalised stress distribution behind the wall. It can be conceived that an increase in the wall roughness results in an increase in the magnitude of σ/γH. Similar to the effect of soil friction, the stress distribution is greatly pronounced at the lower part of the wall for higher wall roughness. The wall roughness was kept constant throughout the height of the wall in this analysis. However, based on the observation from Fig. 10, it can be understood that the lower part of the wall majorly contributes to the mobilisation of the passive resistance offered by the soil. Hence, by improving

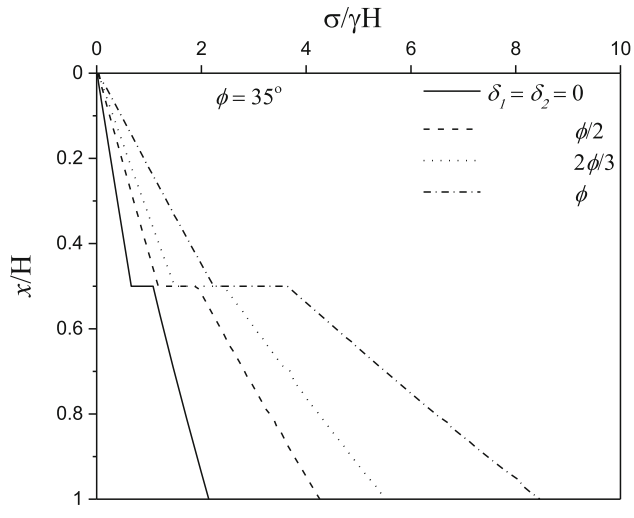

Fig. 10 Normalised stress distribution for different values of δ_1 and δ_2 with $\phi = 35°$, $\alpha_1 = \alpha_2 = 100°$, $H_1/H_2 = 1$, $k_h = 0.2$, $k_v = -0.5k_h$ and $D_S = 10\%$

the roughness of the lower part of the wall, greater stability of the system can be expected. Thus, the present observations from Figs. 9 and 10 conclude that the lower part of a hunchbacked wall contributes more towards the stability aspect of the wall.

4.3.3 Seismic waves

The seismic environment in the analysis was created with the help of MPD approach, where the direction of horizontal and vertical accelerations was chosen to capture the critical condition under the passive state. It was reported in the literature that the detrimental effect of the earthquake

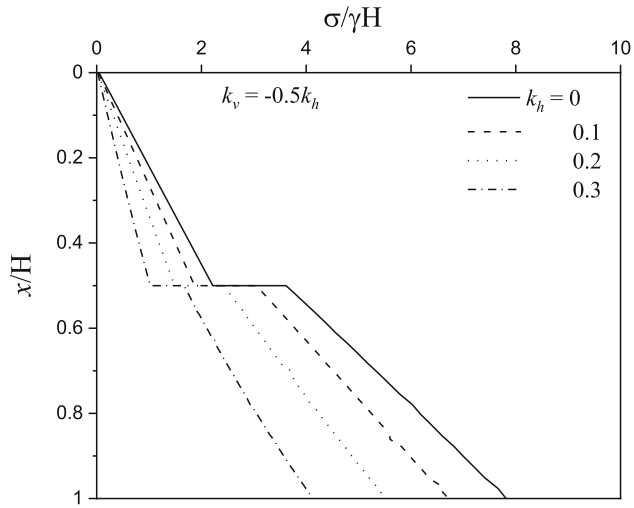

Fig. 11 Normalised stress distribution for different values of k_h with $\phi = 35°$, $\delta_1 = \delta_2 = 2\phi/3$, $\alpha_1 = \alpha_2 = 100°$, $H_1/H_2 = 1$, $k_v = -0.5k_h$ and $D_S = 10\%$

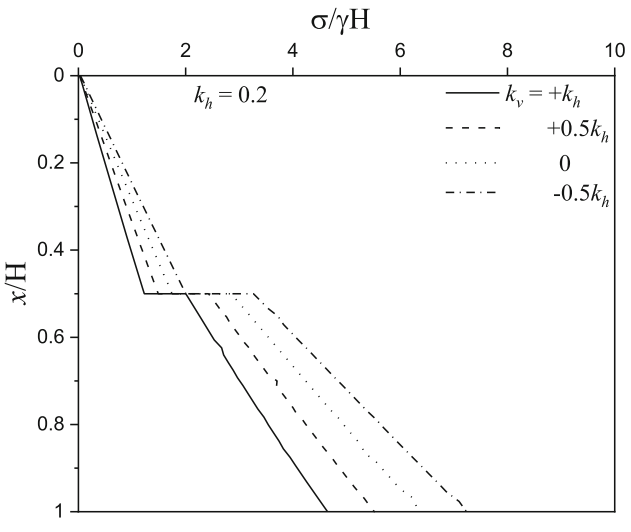

Fig. 12 Normalised stress distribution for different values of k_v with $\phi = 35°$, $\delta_1 = \delta_2 = 2\phi/3$, $\alpha_1 = \alpha_2 = 100°$, $H_1/H_2 = 1$, $k_h = 0.2$ and $D_S = 10\%$

on a retaining structure was majorly due to the propagation of shear waves [50]. Hence, the effect of k_h on the normalised stress distribution along the height of the wall is presented in Fig. 11. The stress on the wall is found to decrease with the increase in k_h, which is in line with the observation made by previous researchers [1, 6, 11, 14, 21, 27, 31, 39, 42]. It is worth noting that the direction of k_h was always kept along the positive y direction to explore the critical condition under the passive state. Though the effect of shear waves is more pronounced in the seismic analysis, the influence of primary waves needs to be considered as well [6]. To capture the critical condition, the direction of k_v was generally considered upward, that is, along the negative x direction. However, the effect of other possible direction of k_v (along the positive x direction) on the stress distribution was also explored as it might be crucial at higher acceleration and different frequency ranges [2]. Hence, the effect of the direction of k_v on the variation of normalised stress is presented in Fig. 12, where it can be observed that at $k_h = 0.2$, $\omega H/$

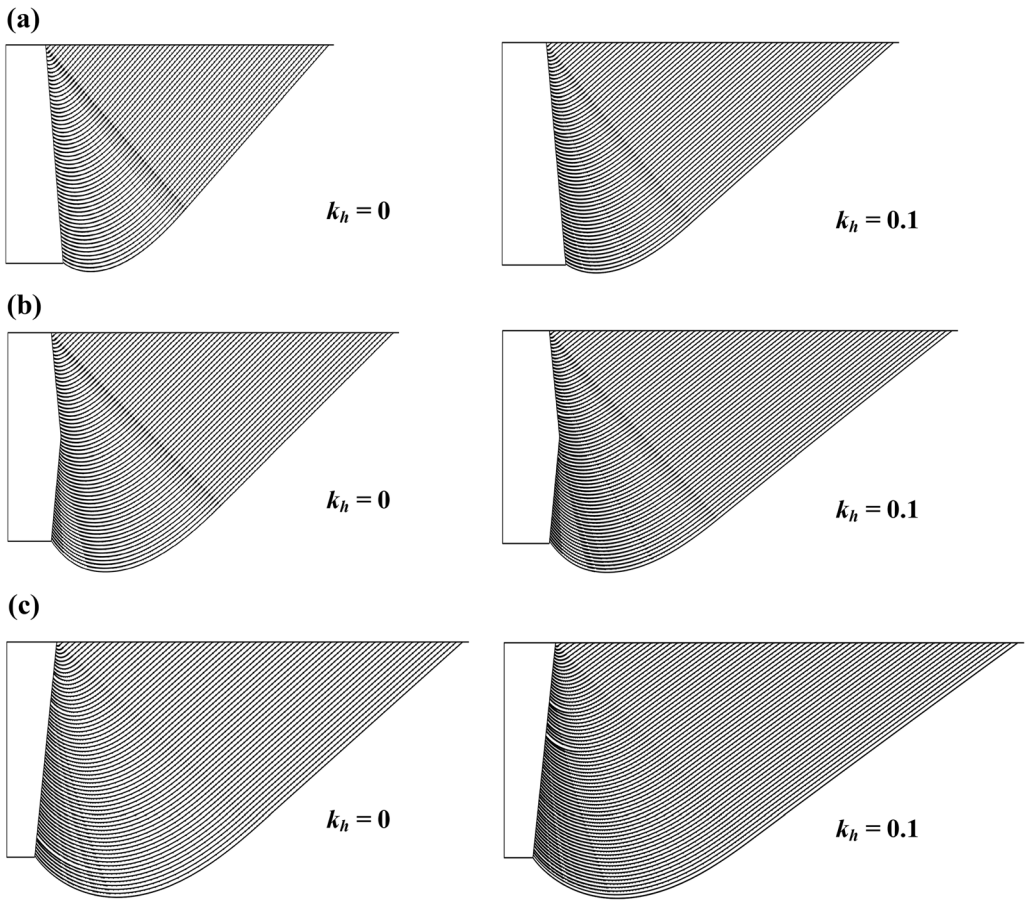

Fig. 13 Failure pattern for different wall configurations under static and seismic conditions with $\phi = 35°$, $\delta_1 = \delta_2 = \phi$, $\alpha_1 = \alpha_2 = 100°$, $k_v = -0.5k_h$ and $D_S = 10\%$; **a** $H_1 = H$, **b** $H_1/H_2 = 1$, **c** $H_2 = H$

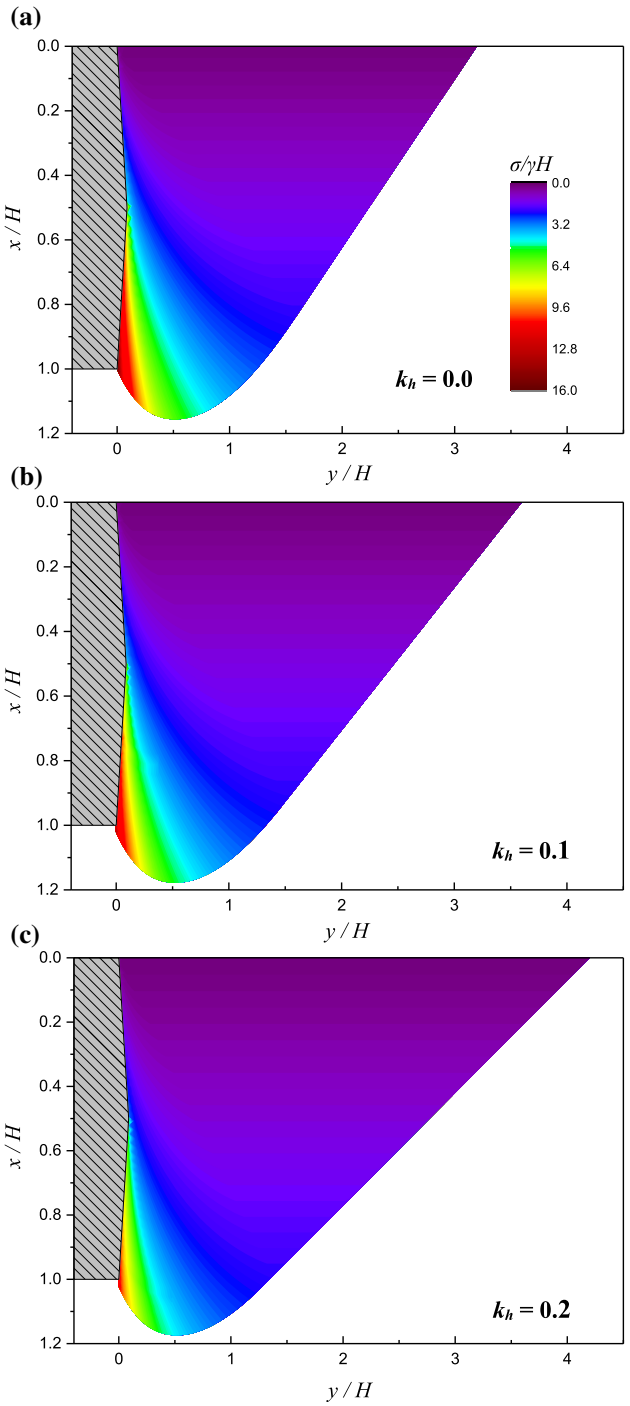

Fig. 14 Normalised stress contours for different values of k_h under static and seismic conditions with $\phi = 35°$, $\delta_1 = \delta_2 = \phi$, $\alpha_1 = \alpha_2 = 100°$, $k_v = -0.5k_h$ and $D_S = 10\%$; **a** $k_h = 0$, **b** $k_h = 0.1$, **c** $k_h = 0.2$

$V_{sS} = 0.95$ and $\omega H/V_{pS} = 0.50$, (σ/γH) decreases as k_v changes its direction from negative (upward) to positive (downward).

4.4 Failure surface

As mentioned earlier, the present methodology needs not to assume any predetermined failure mechanism, and the actual failure surface in the backfill soil evolves automatically from the solution of the method of stress characteristics. Figure 13 depicts typical failure patterns for a hunchbacked as well as a conventional retaining wall with different wall configurations under the static and the seismic conditions. It can be observed from Fig. 13 that for a particular wall configuration, the size of the failure domain increases with an increase in the seismic acceleration. It is worth noting that the size of the failure domain becomes maximum for the conventional wall with $H_2 = H$ (Fig. 13c) and thus provides the highest passive resistance. However, a significant reduction in the consumption of wall material gets ensured in the case of a hunchbacked wall compared to other conventional wall configurations under both static and seismic conditions.

4.5 Stress contours

Since the state of stress is completely known within the influence domain, the mobilisation of stresses within the soil domain can be captured in the form of stress contours. Figure 14 shows the normalised stress contours for a broken-back wall under both static and seismic conditions. It can be observed from Fig. 14 that the magnitude of $\sigma/\gamma H$ generally decreases with an increase in the seismic acceleration. It is worth noting that the rate of reduction is seen to be gradual near the lower part of the wall and hence, the lower segment of the broken-back wall enhances the stability of the wall by providing sufficient passive resistance.

5 Comparison

Under the static and the seismic conditions, a number of studies on the analysis of a conventional linear retaining wall (Fig. 1a) are available in the literature, whereas the same for a hunchbacked retaining wall with bilinear backface (Fig. 1b) are still scarce. Most of the previous studies on a hunchbacked wall were performed using the limit equilibrium method, where a priori rupture surface was assumed. However, the present analysis was carried out considering an adaptive rupture surface along with more appealing MPD approach, which imparted more insight and flexibility to the proposed problem. As virtually no studies related to the passive resistance of a hunchbacked wall are available in the literature, the present analysis was extended to obtain the passive earth pressure coefficients for a conventional vertical retaining wall

Table 2 Comparison of $K_{p\gamma 1}$ for vertical wall under pseudo-static condition with $\phi = 30°$, $\delta_1 = \delta_2 = \phi$, $\alpha_1 = \alpha_2 = 90°$, $H_1 = H$ and $k_v = 0$

k_h	$K_{p\gamma 1}$										
	Mononobe–Okabe method	Morrison and Ebeling [27]	Soubra [42]	Kumar [20]	Kumar and Chitikela [21]	Subba Rao and Choudhury [44]	Mylonakis et al. [28]	Lancellotta [22]	Ganesh and Sahoo [10]	Krabbenhoft [19]	Present study
0.0	10.10	7.08	6.86	6.68	6.56	6.68	5.80	5.03	6.89	5.68	6.51
0.1	9.02	6.66	6.35	6.19	6.08	6.24	5.45	4.70	6.37	5.28	6.05
0.2	7.92	6.15	5.79	5.66	5.56	5.89	5.05	4.29	5.81	4.83	5.53
0.3	6.78	5.54	5.17	5.07	4.99	5.49	4.59	3.81	5.19	4.33	4.97

Table 3 Comparison of $K_{p\gamma 1}$ for vertical wall under OPD condition with $\phi = 30°$, $\delta_1 = \delta_2 = \phi$, $\alpha_1 = \alpha_2 = 90°$, $H_1 = H$, $k_v = 0$, $D_s = 10\%$ and $\omega H/V_{ss} = 1.87$

k_h	$K_{p\gamma 1}$					
	Choudhury and Nimbalkar [6]	Ghosh [11]	Basha and Babu [1]	Ghosh and Kolathayar [14]	Santhoshkumar and Ghosh [40]	Present study
0.0	10.10	10.10	6.60	6.68	5.78	6.51
0.1	9.17	9.17	5.60	6.26	5.52	6.14
0.2	8.23	8.23	4.48	5.82	5.30	5.72

Table 4 Comparison of $K_{p\gamma 1}$ for vertical wall under MPD condition with $\phi = 30°$, $\delta_1 = \delta_2 = \phi$, $\alpha_1 = \alpha_2 = 90°$, $H_1 = H$, $k_v = 0$, $D_s = 10\%$ and $\omega H/V_{ss} = 0.95$

k_h	$K_{p\gamma 1}$				
	Pain et al. [31]	Rajesh and Choudhury [33]	Santhoshkumar and Ghosh [40]	Khatri [17]	Present study
0	6.67	6.67	5.78	6.39	6.51
0.1	5.95	5.95	5.17	5.36	5.80
0.2	5.10	5.11	4.40	3.71	4.95
0.3	4.05	4.05	3.31	2.27	3.87

($H_1 = H$) using different seismic approaches such as pseudo-static, OPD and MPD. In Table 2, the present values of the passive earth pressure coefficient obtained from the pseudo-static approach for a vertical cantilever retaining wall (no wall inertia) are compared with the available studies reported in the literature [10, 19–22, 26–28, 30, 42, 44]. The magnitudes of the seismic passive pressure coefficient reported by Mylonakis et al. [28], Lancellotta [22] and Krabbenhoft [19] are found to be lower than the present values. This may be attributed to the closed form solution proposed by Mylonakis et al. [28] by considering the unit weight component of the soil partially and the lower bound limit analysis solution adopted by Lancellotta [22] and Krabbenhoft [19]. Generally, the results obtained from the method of stress characteristics are reported to lie between the lower and the upper bounds [5]. This observation is quite evident from Table 2, where the present values of the passive earth pressure coefficient fall between the lower [19, 22] and the upper [10, 42] bound results. However, the present results are seen to be in good agreement with that of Kumar and Chitikela [21], where the method of stress characteristics was employed in the analysis. When the current characteristic analysis is coupled with the OPD approach [43], the present results for a vertical retaining wall are generally found to be lower than the available limit equilibrium results [1, 6, 11, 14] based on a predefined failure mechanism (Table 3). The present results are found to be lower than that of Ghosh and Kolathayar [14] though Ghosh and Kolathayar [14] adopted a composite nonlinear failure surface in the analysis. Basha and Babu [1] also considered a composite nonlinear failure surface and reported lower

values of earth pressure coefficient, but their analysis suffered from several limitations as discussed by Ghosh and Kolathayar [14]. However, the closed-form results of Santhoshkumar and Ghosh [40] are found to be the lowest, where the contribution of the unit weight of the soil was completely neglected. Hence, from Table 3, it can be conceived that the present analysis generally reports lower and thus better results among the available studies reported in the literature. In Table 4, the present results for a vertical wall obtained from the MPD approach are compared with that proposed by Pain et al. [31], Rajesh and Choudhury [33], Santhoshkumar and Ghosh [40] and Khatri [17]. It can be observed that the present values of the passive pressure coefficient are lower and thus better than that of Pain et al. [31] and Rajesh and Choudhury [33] though a predefined curved failure surface was considered in their analysis. However, the present results are found to be slightly higher than the lower bound solution of Khatri [17] for the obvious reason.

6 Conclusions

The seismic stability of a hunchbacked retaining wall under the passive state was analysed using the method of stress characteristics in association with the modified pseudo-dynamic approach. While the solution of stress characteristics was able to generate the failure surface automatically along with the complete state of stress in the backfill soil, the MPD approach incorporated the necessary boundary conditions along with the effect of damping and frequency in the analysis. The effect of soil and wall inertia was effectively included in the analysis, which made the study more close to reality. A detailed parametric study was conducted to understand the influence of various parameters such as soil friction, wall roughness, wall backface geometry, seismic accelerations due to shear and primary waves on the seismic pressure distribution behind a hunchbacked wall. The allowable driving force for a hunchbacked wall is found to be 2–7% higher than that of a conventional wall. However, through the application of a hunchbacked wall, there exists a considerable reduction in the construction material along with a marginal improvement in the stability, which strongly advocates for the installation of a hunchbacked retaining wall in place of a conventional wall.

References

1. Basha BM, Babu GLS (2009) Computation of sliding displacements of bridge abutments by pseudo-dynamic method. Soil Dyn Earthq Eng 29(1):103–120
2. Bellezza I (2014) A new pseudo-dynamic approach for seismic active soil thrust. Geotech Geol Eng 32(2):561–576
3. Bellezza I (2015) Seismic active earth pressure on walls using a new pseudo-dynamic approach. Geotech Geol Eng 33(4):795–812
4. Cao W, Liu T, Xu Z (2019) Calculation of passive earth pressure using the simplified principal stress trajectory method on rigid retaining walls. Comput Geotech 109:108–116. https://doi.org/10.1016/j.compgeo.2019.01.021
5. Chen WF (1975) Limit analysis and soil plasticity. Elsevier, Amsterdam
6. Choudhury D, Nimbalkar S (2005) Seismic passive resistance by pseudo-dynamic method. Géotechnique 55(9):699–702
7. Coulomb CA (1773) Sur une application des regles de maximis et minimis a quelques problemes de statique relatifs a l'architecture. Mem Math Phys par Divers Savants
8. Das BM (1993) Principles of soil dynamics. PWS-KENT, Boston, USA
9. European Committee for Standardization (CEN) (2004) Eurocode 8: Design of structures for earthquake resistance–Part 5: foundations, retaining structures and geotechnical aspects. Ref. No. EN 1998–5:2004, CEN, Brussels, Belgium
10. Ganesh R, Sahoo JP (2017) Seismic passive resistance of cohesive-frictional soil medium: kinematic limit analysis. Int J Geomech 17(8):04017029–1–26
11. Ghosh P (2007) Seismic passive earth pressure behind non-vertical retaining wall using pseudo-dynamic analysis. Geotech Geol Eng 25(1):117–123
12. Ghosh P (2008) Upper bound solutions of bearing capacity of strip footing by pseudo-dynamic approach. Acta Geotech 3(2):115–123
13. Ghosh P (2009) Seismic vertical uplift capacity of horizontal strip anchors using pseudo-dynamic approach. Comput Geotech 36(1–2):342–351
14. Ghosh P, Kolathayar S (2011) Seismic passive earth pressure behind non vertical wall with composite failure mechanism: pseudo-dynamic approach. Geotech Geol Eng 29(3):363–373
15. Guojun X, Jianhua W (2018) A rigorous characteristic line theory for axisymmetric problems and its application in circular excavations. Acta Geotech. https://doi.org/10.1007/s11440-018-0697-7
16. Indian Standard (IS) 1893(2014): Indian standard criteria for earthquake resistant design of structures. Part 3: Bridges and retaining walls. Bureau of Indian Standards, New Delhi
17. Khatri VN (2019) Determination of passive earth pressure with lower bound finite elements limit analysis and modified pseudo-dynamic method. Geomech Geoengin. https://doi.org/10.1080/17486025.2019.1573324
18. Kolathayar S, Ghosh P (2011) Seismic passive earth pressure on walls with bilinear backface using pseudo-dynamic approach. Geotech Geol Eng 29(3):307–317
19. Krabbenhoft K (2018) Static and seismic earth pressure coefficients for vertical walls with horizontal backfill. Soil Dyn Earthq Eng 104:403–407
20. Kumar J (2001) Seismic passive earth pressure coefficients for sands. Can Geotech J 38(4):876–881
21. Kumar J, Chitikela S (2002) Seismic passive earth pressure coefficients using the method of characteristics. Can Geotech J 39(2):463–471
22. Lancellotta R (2007) Lower-bound approach for seismic passive earth resistance. Géotechnique 57(3):319–321
23. Lee IK, Herington JR (1972) A theoretical study of the pressures acting on a rigid wall by a sloping earth or rock fill. Géotechnique 22(1):1–26

24. Li C, Jiang P, Zhou A (2019) Rigorous solution of slope stability under seismic action. Comput Geotech 109:99–107. https://doi.org/10.1016/j.compgeo.2019.01.018
25. Lin Y-L, Yang X, Yang G-L et al (2017) A closed-form solution for seismic passive earth pressure behind a retaining wall supporting cohesive–frictional backfill. Acta Geotech 12(2):453–461
26. Mononobe N, Matsuo H (1929) On the determination of earth pressure during earthquake. In: Proceedings of the World Engineering Conference. pp 177–185
27. Morrison EE, Ebeling RM (1995) Dynamic passive earth pressure. 487(3):481–487
28. Mylonakis G, Kloukinas P, Papantonopoulos C (2007) An alternative to the Mononobe-Okabe equations for seismic earth pressures. Soil Dyn Earthq Eng 27(10):957–969
29. Newmark NM (1965) Effects of earthquakes on dams and embankments. Géotechnique 15(2):139–160
30. Okabe S (1926) General theory of earth pressure. J Japan Soc Civ Eng 12(1):311
31. Pain A, Choudhury D, Bhattacharyya SK (2017) Seismic passive earth resistance using modified pseudo-dynamic method. Earthq Eng Eng Vib 16(2):263–274
32. PIANC (2001) Seismic design guidelines for port structures. International Navigation Association. A. A, Balkema, Tokyo
33. Rajesh BG, Choudhury D (2017) Seismic passive earth resistance in submerged soils using modified pseudo-dynamic method with curved rupture surface. Mar Georesources Geotechnol 35(7):930–938
34. Rajesh BG, Choudhury D (2018) Seismic stability of seawalls under earthquake and tsunami forces using a modified pseudo-dynamic method. Nat Hazards Rev 19(3):04018005–1–12
35. Rankine WJM (1857) On the stability of loose earth. Philos Trans R Soc London 147:9–27
36. Richards R, Elms DG, Budhu M (1990) Dynamic fluidization of soils. J Geotech Eng 116(5):740–759
37. Sadrekarimi A, Ghalandarzadeh A, Sadrekarimi J (2008) Static and dynamic behavior of hunchbacked gravity quay walls. Soil Dyn Earthq Eng 28(2):99–117
38. Sadrekarimi A (2017) Seismic distress of broken-back gravity retaining walls. J Geotech Geoenvironmental Eng 143(4):04016118
39. Santhoshkumar G, Ghosh P (2018) Seismic passive earth pressure on an inclined cantilever retaining wall using method of stress characteristics – A new approach. Soil Dyn Earthq Eng 107:77–82
40. Santhoshkumar G, Ghosh P (2019) Closed-form solution for seismic earth pressure on bilinear retaining wall using method of characteristics. J Earthq Eng. https://doi.org/10.1080/13632469.2019.1570880
41. Sokolovski VV (1960) Statics of Soil Media, 2nd edn. Butterworths Scientific Publications, London
42. Soubra AH (2000) Static and seismic passive earth pressure coefficients on rigid retaining structures. Can Geotech J 37(2):463–478
43. Steedman RS, Zeng X (1990) The influence of phase on the calculation of pseudo-static earth pressure on a retaining wall. Géotechnique 40(1):103–112
44. Subba Rao KS, Choudhury D (2005) Seismic passive earth pressures in soils. J Geotech Geoenvironmental Eng 131(1):131–135
45. Sun Y, Song E (2016) Active earth pressure analysis based on normal stress distribution function along failure surface in soil obeying nonlinear failure criterion. Acta Geotech 11(2):255–268
46. USBR (1976) Design of gravity dams. United States Department of the Interior, A Water Resources Technical Publication, Denver, Colorado
47. Wilson PR (2009) Large scale passive force-displacement and dynamic earth pressure experiments and simulations. University of California, San Diego
48. Xu S-Y, Kannangara KKPM, Taciroglu E (2018) Analysis of the stress distribution across a retaining wall backfill. Comput Geotech 103:13–25
49. Xu S-Y, Lawal AI, Shamsabadi A, Taciroglu E (2019) Estimation of static earth pressures for a sloping cohesive backfill using extended Rankine theory with a composite log-spiral failure surface. Acta Geotech 14:579–594
50. Zeng X, Steedman RS (1993) On the behaviour of quay walls in earthquakes. Géotechnique 43(3):417–431